Hindawi
Scientific Programming
Volume 2021, Article ID 7880477, 12 pages
https://doi.org/10.1155/2021/7880477

Research Article

Machine Learning-Based Head Computerized Tomography Imaging in Diagnosis and Surgery Treatment of Hypertension Cerebral Hemorrhage

Jinjiang Dong and Jianhao Mao

Department of Neurosurgery, The First People's Hospital of Chun'an County, Hangzhou 311700, Zhejiang, China

Correspondence should be addressed to Jianhao Mao; 1608401012@stu.suda.edu.cn

Received 28 August 2021; Revised 29 September 2021; Accepted 1 October 2021; Published 20 October 2021

Academic Editor: Gustavo Ramirez

The aim of this study was to explore the adoption of computerized tomography (CT) based on machine learning in the diagnosis and treatment of cerebral hemorrhage. A total of 150 patients with hypertensive intracerebral hemorrhage who underwent surgical treatment in hospital in the recent three years were selected. All patients underwent brain CT examination, and image data were collected. FCM, DRLSRE, FCRLS, and other algorithms were utilized to segment the patient's bleeding region, and the segmentation performance of each algorithm was compared. Based on the FCRLS algorithm segmentation, the bleeding area was calculated by using the function in the MATLAB toolbox. Based on the previous research, a computer-aided diagnosis (CAD) system was designed and verified. The results showed that FCRLS had the best segmentation effect and the fastest segmentation speed for discontinuous and irregular bleeding areas. The CAD system can obtain the information of bleeding site, bleeding amount, midline displacement, and ventricle compression comprehensively and accurately. The accuracy of this system was 94% and 86% for hematoma of patients with rapid bleeding and those with slow bleeding, respectively. The overall accuracy was 91.3%. To sum up, the CAD system based on machine learning and head CT image had good diagnostic effect for patients with hypertensive intracerebral hemorrhage and had high clinical adoption value.

1. Introduction

Hypertensive intracerebral hemorrhage is a common disease of spontaneous intracerebral hemorrhage with high mortality and disability in the world. Intracerebral hemorrhage is mostly caused by capillary rupture of the brain, cerebellum, and brainstem [1]. The common vascular disease changes into fibrous and hyaline vascular wall, which further leads to local ischemic necrosis of the vascular wall. At that time, the vessel wall will exhibit localized dilation and aneurysm will appear, and when the blood pressure fluctuates too much, the vessel rupture will occur [2–4]. Anything that can cause blood pressure to fluctuate too much can cause blood pressure to bleed, such as excessive happiness, sadness, long hours of work, and severe mental and physical exhaustion, which may all lead to the sudden rupture of an already diseased blood vessel. Clinical data showed that the probability of hypertensive hemorrhage in the putamen, subcutaneous layer of cerebral lobes, thalamus, pons, and cerebellum were 15.1%, 55.3%, 10.04%, 10.01%, 10.11%, and 10.1%, respectively [5]. After hypertensive hemorrhage, the damage to the brainstem, especially the hypothalamus, is great, which often leads to central pulmonary edema, respiratory disorders, acute gastrointestinal bleeding, and brain-heart syndrome. These complications are extremely averse to the prognosis of patients, and more serious cases will directly cause the death of patients. In short, hypertensive cerebral hemorrhage poses a great threat to people's life and health [6].

At present, one of the important bases for doctors to make treatment plan for patients with intracerebral hemorrhage is the image of computed tomography (CT) and the clinical manifestations of patients. Doctors often need to obtain the bleeding site, bleeding amount, midline

displacement, and ventricle compression degree from CT diagnostic images of intracerebral hemorrhage. These are important indicators of whether patients need to undergo craniotomy according to the diagnostic knowledge of hemorrhage surgery [7]. At present, most domestic hospitals still rely on the traditional Tada equation to calculate the amount of cerebral hemorrhage by hand, which has many shortcomings such as tedious, low efficiency, and poor repeatability. In addition, clinical statistics showed that the calculation error of hematoma volume by this method was as high as 17.32%, especially for lobulated group (discontinuous boundary bleeding area), the calculation error rate was as high as 38.27% ± 11.33%. The calculation of error rate is as follows: error rate = (the amount of intracerebral hemorrhage obtained by Tada's equation − the amount obtained by 3D slicer software)/the amount obtained by 3D slicer software. In addition, the clinician observed the cranial CT images of the patients by naked eye with the PACS influence browsing system and diagnosed the midline displacement and the degree of ventricular compression of the patients based on personal experience. It often leads to inaccurate diagnostic information and even misdiagnosis and missed diagnosis, as well as inconsistent diagnostic results among different doctors for the same patient [8]. At present, there are four common treatment methods for hypertensive hemorrhage, including conservative drug treatment, minimally invasive surgical treatment, stereotactic intracerebral hematoma drainage, and craniotomy and bone flap removal. Studies showed that the amount of intracranial residual hematoma and the rate of absorption of hematoma are closely related to the recovery of neurological function in the course of conservative treatment. However, the information is mostly obtained by CT images. In short, craniocerebral CT plays a very important role in the diagnosis, treatment, and prognosis of hypertensive cerebral hemorrhage. The current calculation methods of cerebral hemorrhage and reading are not accurate. In addition, with the more and more extensive clinical adoption of CT, the reading pressure of doctors is constantly increasing [9]. Therefore, it is very necessary to develop a set of auxiliary diagnosis systems based on CT images for patients with hypertensive bleeding. FCRLS algorithm can calculate the volume of irregular hematoma accurately. The system also includes CT image preprocessing, segmentation of focal area, acquisition of diagnostic information, and prediction of hematoma absorption speed.

With the continuous development of Internet technology, computer-aided diagnosis (CAD) is widely utilized in the medical field. Compared with the traditional diagnostic calculation, using CAD to process and analyze images can reduce the pressure on doctors to read images, and it can improve the accuracy and efficiency of diagnosis. In addition, it can also avoid the occurrence of different diagnostic results caused by the limitation of doctors' experience and knowledge level, which is of great significance to the improvement of medical level [10]. At present, there is a certain gap in the research of related issues in China, and foreign countries are ahead of domestic ones. The precise segmentation of bleeding area in CT images has been studied by many foreign scholars. However, most of them are based on theoretical analysis, which is quite different from the actual situation and their practicability needs to be improved in solving the practical problems in clinical practice. The 3D slicer software, jointly developed by the Palmistry Planning Laboratory at Women's Hospital Boston and the Artificial Intelligence Laboratory at the Massachusetts Institute of Technology (MIT), was released in version 4.2 in 2012. The software is not restricted by bleeding site and hematoma shape, and its adoption is gradually mature. Domestic research is relatively backward, and some scholars proposed CT volume measurement to measure hematoma volume [11]. This method is not affected by hematoma volume, and the measurement result is accurate. However, both hematoma volume and 3D reconstruction need to be done on the CT table. Some scholars proposed methods to try to measure hematoma volume, but if the method needs to obtain the final hematoma volume, it needs to be further calculated with the help of equations. In general, cerebral hemorrhage CAD research results are relatively more in the field of CAD. However, the diagnostic system has many problems, such as single function, limited information that doctors can get from the diagnostic system, and low value in clinical practice. In addition, most existing systems can only segment regular and continuous high-density areas, but cannot segment discontinuous, irregular, and invisible lesion areas [12]. With the development of Internet technology, computer-aided diagnostic medicine has been developed. Machine learning algorithms are widely used. The machine learning algorithm in this work includes calculation of the proportion of bleeding area. The binarization processing is performed on CT images of cerebral hemorrhage after segmentation by FCRLS algorithm and calculation of slice area of monolayer CT. In this work, based on machine learning theory, a CAD system was established with CT images of patients with hypertensive intracerebral hemorrhage as research data, to provide reference and basis for related research.

2. Methods

2.1. Collection of CT Image Data. A total of 150 patients with hypertensive cerebral hemorrhage admitted to hospital from January 2017 to November 2019 were selected as the research objects. The diagnosis of all subjects was based on the diagnostic criteria, clinical symptoms, and CT images of cerebrovascular diseases defined in the "National Cerebrovascular Disease Academic Conference of the Chinese Medical Association" in 1995. Exclusion criteria were as follows: patients with primary intraventricular hemorrhage, patients with subarachnoid hemorrhage, patients with arteriovenous malformation, patients with cerebral hemorrhage caused by intracranial aneurysm, patients with traumatic cerebral hemorrhage, patients with intracerebral hemorrhage caused by other causes after thrombolytic therapy, and patients with severe infection and high fever did not retreat.

2.2. Methods of Distinguishing between Different Groups. Acute intracerebral hemorrhage is a series of acute clinical symptoms caused by the rapid rupture of cerebrovascular soil. They often show symptoms such as severe headache, vomiting, limb paralysis, and even coma. Chronic intracerebral hemorrhage generally refers to the pathological changes of blood vessel itself, or the pathological changes of blood system itself, leading to the disorder of blood coagulation mechanism of patients, mild rupture of cerebrovascular, slow bleeding speed, long bleeding time, or intracerebral hemorrhage caused by hemodialysis for a long time in brain tissue.

2.3. Segmentation Algorithm of Irregular, Discontinuous, and Unobvious Bleeding Region. The spatial fuzzy C-means clustering segmentation algorithm (FCM) is derived from the K-means clustering algorithm.

$$J = \sum_{m=1}^{K} \sum_{n=1}^{N} \left\| i_n - v_m \right\|^2. \tag{1}$$

The objective function of FCM algorithm is similar to equation (1).

$$J = \sum_{n=1}^{N} \sum_{m=1}^{C} u_{mn}^{l} \left\| i_n - v_m \right\|^2. \tag{2}$$

In equation (2), l is the weight index acting on fuzzy slavery degree, C is the number of clustering categories, and u_{mn} is an algorithm member function.

$$\begin{gathered} \forall m, n, \\ \sum_{m=1}^{c} u_{mn} = 1, \\ u_{mn} \in [0, 1], \\ \sum_{n=1}^{N} u_{mn} > 0. \end{gathered} \tag{3}$$

The member function u_{mn} and cluster center function V_m can be solved by the following equation:

$$u_{mn} = \frac{\left\| i_n - v_m \right\|^{-2/(l-1)}}{\sum_{K=1}^{C} \left\| i_n - v_k \right\|^{-2/(l-1)}}, \tag{4}$$

$$V_m = \frac{\sum_{n=1}^{N} u_{mn}^{l} i_n}{\sum_{n=1}^{N} u_{mn}^{l}}. \tag{5}$$

Fuzzy C-means clustering (S_FCM) algorithm based on spatial domain adds spatial domain information to the member function, which is shown as follows:

$$u_{mn} = \frac{u_{mn}^{p} h_{mn}^{q}}{\sum_{K=1}^{C} u_{kn}^{p} h_{kn}^{p}}. \tag{6}$$

In equation (6), p and q are the control parameters of the contribution value of the spatial domain information function h_{mn}^{q} and the traditional member function u_{mn} to the improved member function value u_{mn}. h_{mn}^{q} is a spatial domain function containing the membership degree of domain pixels constructed:

$$h_{mn}^{q} = \sum_{k \in N_n} u_{kn}. \tag{7}$$

The spatial function expression is substituted into equation (5) to update fuzzy membership.

Spatial fuzzy horizontal semiautomatic segmentation algorithm: the equation of single potential hydrazine function is as follows:

$$R_p(\varnothing) \overset{A}{=} \int_{\Omega} p(|\nabla \varnothing|) \mathrm{d}x, \tag{8}$$

$$p(x) = \frac{1}{2}(x-1)^2. \tag{9}$$

Equation (8) indicates that the distance regularized item expression (9) has a unique minimum point $x = 1$. According to the gradient descent flow equation, there is the following equation:

$$\frac{\partial \varnothing}{\partial t} = \varnothing \operatorname{div}\left(d_p(|\nabla \varnothing|) \nabla \varnothing \right). \tag{10}$$

The DRLSE model uses double-well function to improve the distance regularization term, and the double-well function is expressed as follows:

$$P_2(x) \overset{\Delta}{=} \begin{cases} \dfrac{1}{(2\pi)^2}(1 - \cos(2\pi x)), & x \le 1, \\ \dfrac{1}{2}(x-1)^2, & x \ge 1. \end{cases} \tag{11}$$

The energy functional adopted by the DRLSE model for image segmentation is as follows:

$$\varepsilon(\varnothing) = \mu R_p(\varnothing) + \lambda L_g(\varnothing) + \nu A_g(\varnothing). \tag{12}$$

In equation (12), μ, λ, and ν are the coefficients of each energy term, respectively. $uR_p(\varnothing)$ is the internal energy term, and terms 2 and 3 are external energy terms.

$$L_g(\varnothing) = \int_{\Omega} g \delta(\varnothing) |\nabla \varnothing| \mathrm{d}x \mathrm{d}y, \tag{13}$$

$$A_g(\varnothing) = \int_{\Omega} g H(-\varnothing) \mathrm{d}x \mathrm{d}y. \tag{14}$$

In equation (13), g is the edge indicator function, $\delta(x)$ is the Dirac function, and $H(x)$ is Heaviside function, and the DRLSE model defines Heaviside function as follows:

$$H_{\varepsilon}(x) = \begin{cases} \dfrac{1}{2}\left(1 + \dfrac{x}{\varepsilon} + \dfrac{1}{\pi}\sin\left(\dfrac{\pi x}{\varepsilon}\right)\right), & |x| \le \varepsilon, \\ 1, & x > \varepsilon, \\ 0, & x < -\varepsilon. \end{cases} \tag{15}$$

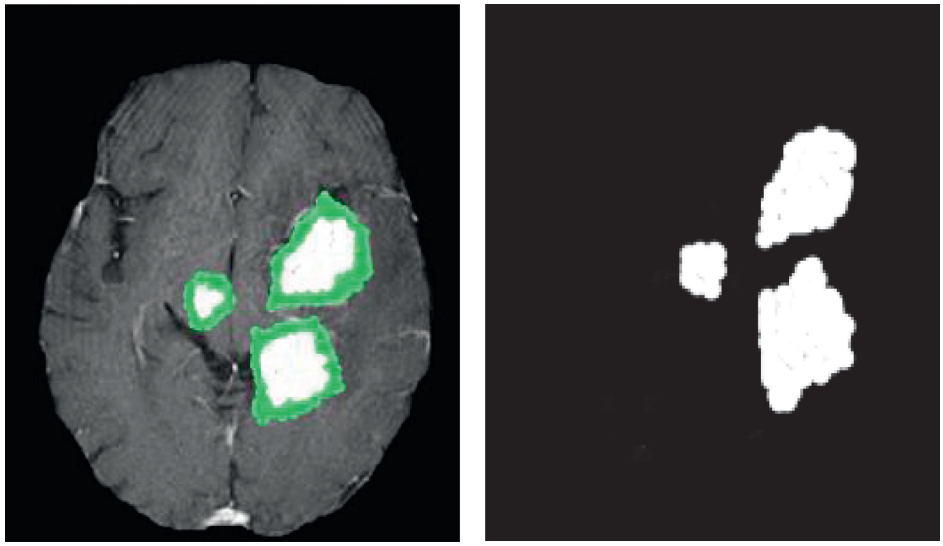

(a) (b)

Figure 1: Binarization of bleeding area after algorithm segmentation. (a) FCRLS algorithm iterative segmentation result and (b) binarization result.

Equations (8), (11), and (13)–(15) are substituted into equation (12), and the energy function expression is rewritten as follows:

$$\varepsilon(\phi) = u\int_{\Omega} p_2(|\nabla\phi|)\mathrm{d}x + \lambda\int_{\Omega} g\delta_{\varepsilon}(\phi)(|\nabla\phi|)\mathrm{d}x + v\int_{\Omega} gH_{\varepsilon}(-\phi)\mathrm{d}x. \tag{16}$$

The Gateaux derivative is utilized to take the derivative of ϕ.

$$\frac{\partial\phi}{\partial t} = u\,\mathrm{div}\left(d_{p2}(|\nabla\phi|)\nabla\phi\right) + \lambda\delta_{\varepsilon}(\phi)\mathrm{div}\left(g\frac{\nabla\phi}{|\nabla\phi|}\right) + vg\delta_{\varepsilon}(\phi). \tag{17}$$

In equation (17), $d_{p2}(x)$ is the first derivative of the function $p_2(x)$:

$$d_{p2}(x) \triangleq \frac{p_2(x)}{x}. \tag{18}$$

Then, the solution is discretized:

$$\phi^{k+1}(x+y) = \phi^{k}(x+y) + \tau\left[u\,\mathrm{div}\left(d_{p2}\left(\left|\nabla\phi^{n}\right|\nabla\phi^{n}\right)\right) + \lambda\delta_{\varepsilon}\left(\phi^{k}\right)\mathrm{div}\left(g\frac{\nabla\phi^{k}}{\left|\nabla\phi^{k}\right|}\right) + vg\delta_{\varepsilon}\left(\phi^{k}\right)\right]. \tag{19}$$

2.4. Calculation of the Amount of Cerebral Hemorrhage. The calculation method of irregular hematoma volume is as follows: (1) calculation of the proportion of bleeding area: binarize the segmented CT image. MATLAB toolbox function graythresh is utilized to obtain the binarization threshold, and then the MATLAB toolbox function im2bw is utilized to convert the gray image into a binary image. The image after the binarization process contains a total of two parts, the bleeding area and the background. The specific binarization process is shown in Figure 1. The specific program syntax is [T, S, M] = graythresh(f): BW = im2bw(I, T).

After the binarization of the CT image, the MATLAB toolbox function bwarea is utilized to calculate the number of pixels in the bleeding area num. After that, the MATLAB toolbox function numel is utilized to calculate the total number of pixels in the CT image after binarization. The proportion of bleeding area is ratio = num/total. The specific calculation flowchart is shown in Figure 2.

(2) Single-slice CT slice area calculation: with 60 patients' brain CT images as research data, the length and width of single-slice CT slices are measured through the measurement tool in the PACS image browser. During the measurement, the measurement objects are randomly selected and the 50 sets of data are averaged at the end of the measurement. The average length and width of the CT slice of cerebral hemorrhage were 23.88 cm and 24.21 cm, respectively. The single-slice CT area is $S = 23.88 \times 24.21 = 578\ \mathrm{cm}^2$. The specific schematic diagram of the measurement of the length and width of the CT slice of cerebral hemorrhage is shown in Figure 3.

The specific calculation equation is obtained by substituting the above parameters into the following equation:

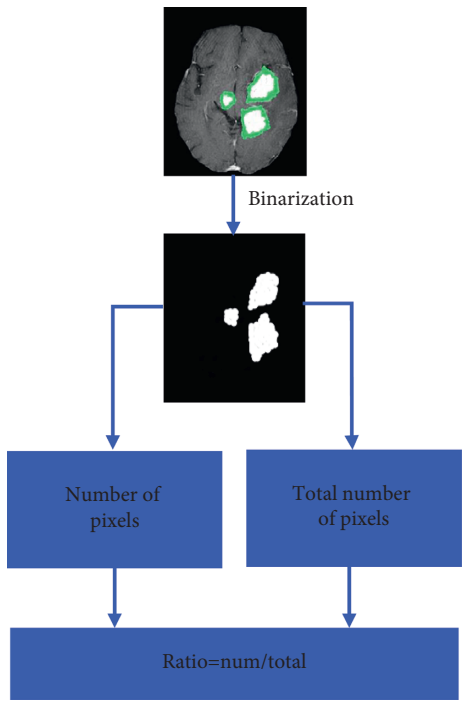

Figure 2: Flowchart of calculation of the proportion of bleeding area.

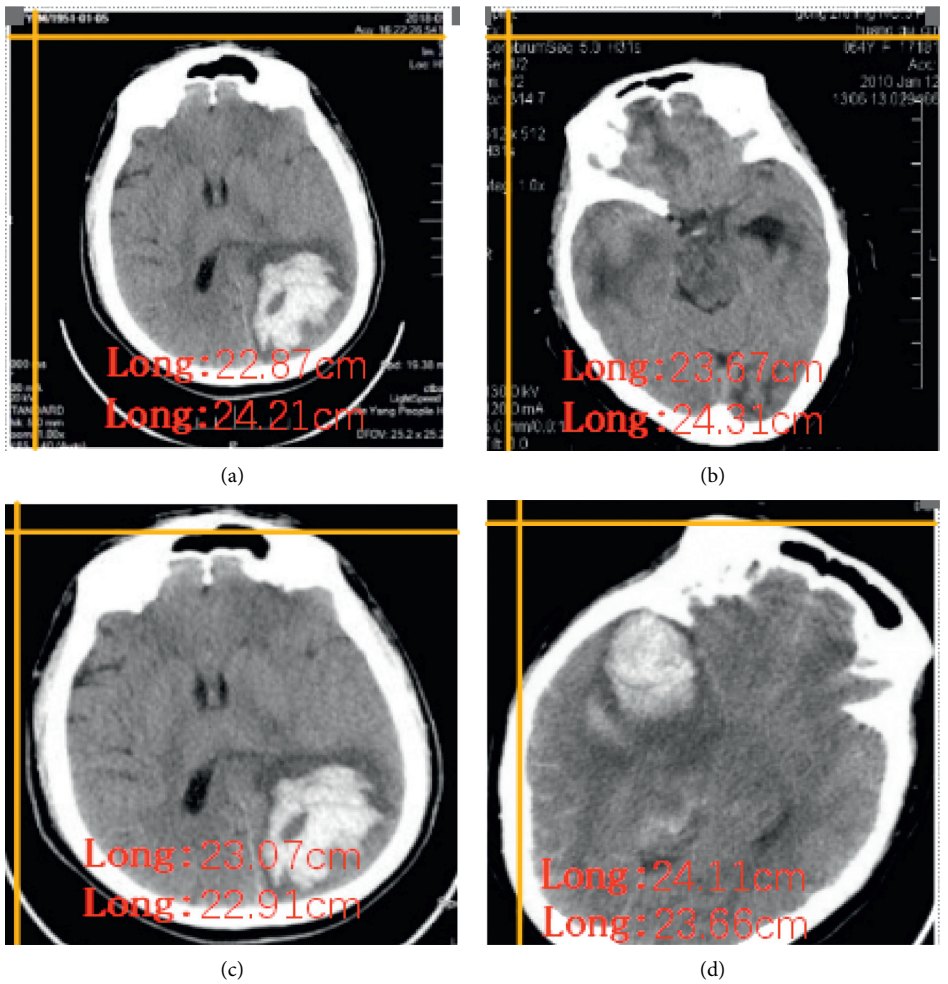

(a) (b) (c) (d)

Figure 3: Schematic diagram of measurement of the length and width of the CT slice of cerebral hemorrhage. (a) Example 1: the length is 22.87 cm and the width is 22.42 cm. (b) Example 2: the length is 23.67 cm and the width is 24.31 cm. (c) Example 3: the length is 23.07 cm and the width is 22.91 cm. (d) Example 4: the length is 24.11 cm and the width is 23.66 cm.

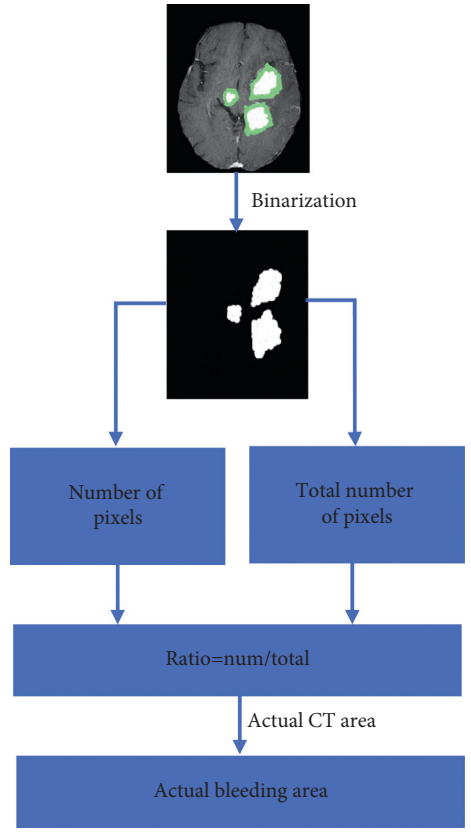

Figure 4: Flowchart of calculation of irregular hematoma volume.

$$V_{\text{Irregular}} = \sum_{i=1}^{N} \text{Ratio}_i \times S \times d. \tag{20}$$

In equation (20), N is the total number of cerebral CT in the bleeding area, Ratio_i is the proportion of CT bleeding area in cerebral hemorrhage, and d is the thickness of single CT layer. The thickness of conventional plain CT scan of cerebral hemorrhage is 1 cm, S is a fixed value ($S = 578\ \text{cm}^2$), and the unit of hematoma volume is mL. The specific calculation flowchart is shown in Figure 4.

The program is implemented as follows:

(i) IMA = reshape(MF(nopt,:,:), size(IM,2); size(IM,2); % Image matrix after FCRLS algorithm segmentation%

(ii) [T, S, M] = graythresh(IMA); % Get global binarization threshold %

(iii) IMM = im2bw(IMA,T); % Convert grayscale image to binary image %

(iv) imshow(IMM,[]); % Display the binarized image %

(v) total = numel(IMM); % Total number of pixels in CT image %

(vi) num = bwarea(IMM); % Number of pixels in bleeding area %

(vii) Ratio = num/total; % Proportion of bleeding area %

(viii) S=Ratio ∗ 23.88 ∗ 24.21% Area of bleeding area in single-slice CT image %

Regular hematoma volume calculation was as follows. (1) A point in the presegmented image was selected as the growth point. (2) Based on the seed region, it was incorporated into the adjacent pixel points with certain regularity. (3) Similar pixel points in this region were merged into the same region. Th = 50, the four adjacent points of the growing points above, below, left, and right were examined. If the difference between the gray value of the adjacency points and the initial growth point was less than the growth threshold, the adjacency point can be merged. The merged pixels were the new "starting point of growth," and then the other four points were investigated and so on until the bleeding area was fully identified. The specific algorithm flowchart is shown in Figure 5.

The number of pixels num in the bleeding area is calculated through the MATLAB toolbox function bwarea. After that, the number of binarized CT images containing all pixels total is calculated by the MATLAB toolbox function numel. The proportion of the bleeding area is calculated as ratio = num/total; the equation for calculating the volume of the regular hematoma is as follows:

$$V_{\text{Regular}} = \sum_{i=1}^{N} \text{ratio}_i \times S \times d. \tag{21}$$

The calculation process of regular hematoma is shown in Figure 6.

The program is implemented as follows:

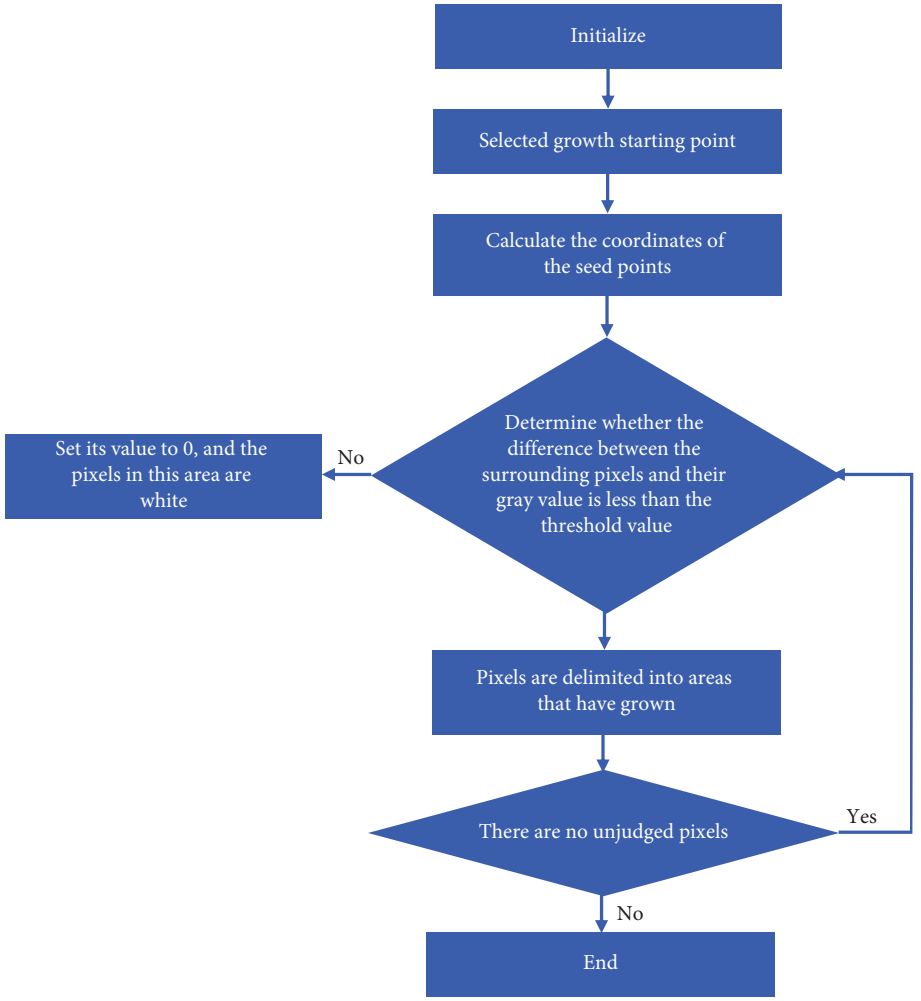

Figure 5: Segmentation flowchart based on the threshold region growing algorithm.

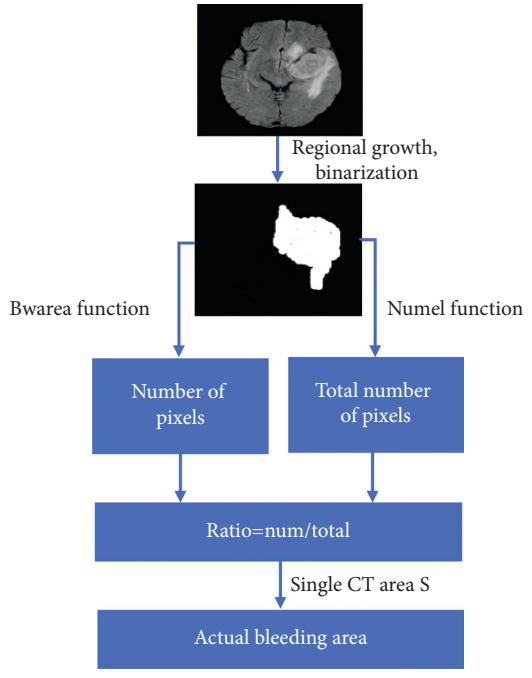

Figure 6: The calculation process of regular hematoma.

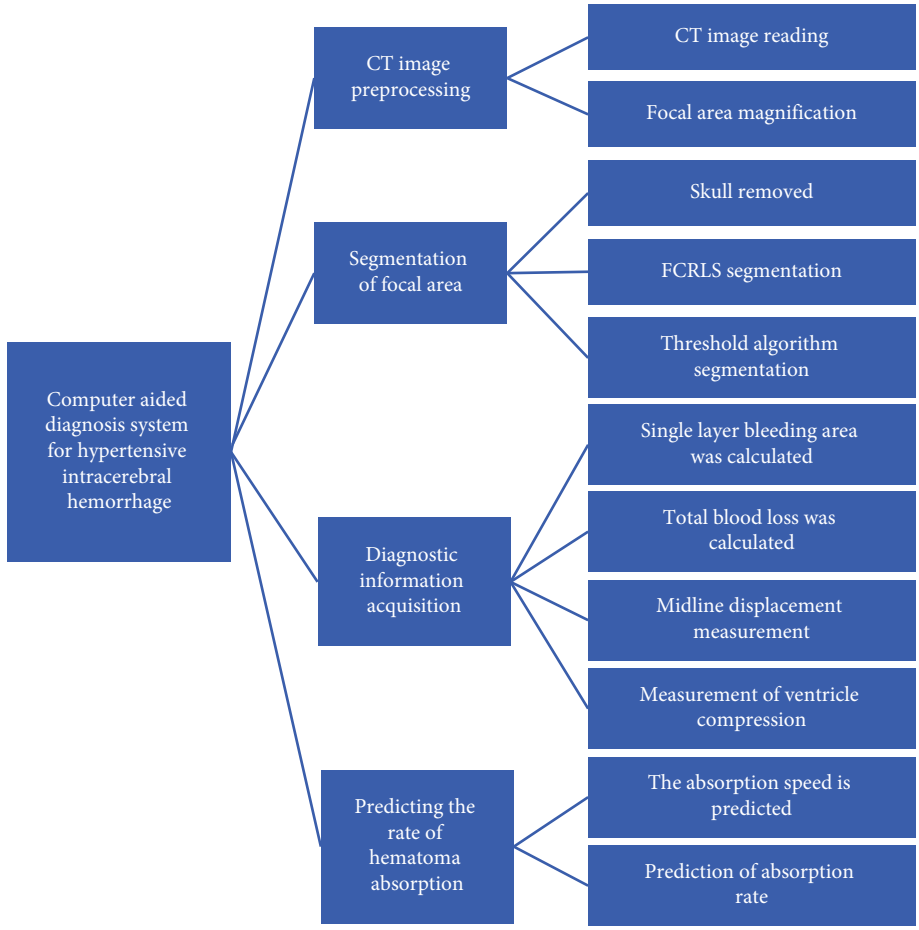

Figure 7: Structure and function diagram of the diagnosis system.

(i) Yout = regiongrow(f,seed,th,_mean); % Image matrix segmented by region growing method %

(ii) Level = graythresh(Yout); % Get global binarization threshold %

(iii) IMM = im2bw(Yout,level); % Convert grayscale image to binary image %

(iv) total = numel(IMM); % Total number of pixels in CT image %

(v) num = bwarea(IMM); % Number of pixels in bleeding area %

(vi) ratio = num/total; % Proportion of bleeding area %

(vii) S = ratio $*$ 23.88 $*$ 24.21% Area of bleeding area in single-slice CT image %

2.5. Design of Computer-Aided System for Hypertensive Cerebral Hemorrhage. Based on the algorithm mentioned above, a CAD system for hypertensive intracerebral hemorrhage was independently developed by using the GUI platform of MATLAB. It consists of four modules of CT image preprocessing, segmentation of lesion area, acquisition of diagnostic information, and prediction of hematoma absorption speed. CT image preprocessing is divided into three parts of cerebral hemorrhage CT image processing, CT image amplification, and skull removal. The segmentation part of the lesion region includes two parts of FCRLS and threshold algorithm segmentation module. The segmentation module of FCRLS algorithm can segment the irregular, nonobvious, and discontinuous bleeding area. Part of the main function of threshold segmentation algorithm is segmenting regular bleeding region. Diagnostic information acquisition consists of four parts of single-layer CT image bleeding area calculation, total bleeding input, midline shift measurement, and ventricle compression change measurement. Hematoma absorption is predicted by the speed of hematoma absorption and the average rate of hematoma absorption. The specific system function structure is shown in Figure 7.

2.6. The Calculation Method of Overall Prediction Accuracy. Prediction accuracy = 1 − (absolute error/predicted demand $*$ 100%). Error absolute value = |actual demand − demand prediction|.

3. Results

3.1. Segmentation Results of Brain CT Images by Various Algorithms. The segmentation results of each algorithm are shown in Figure 8. Combined with the judgments of two

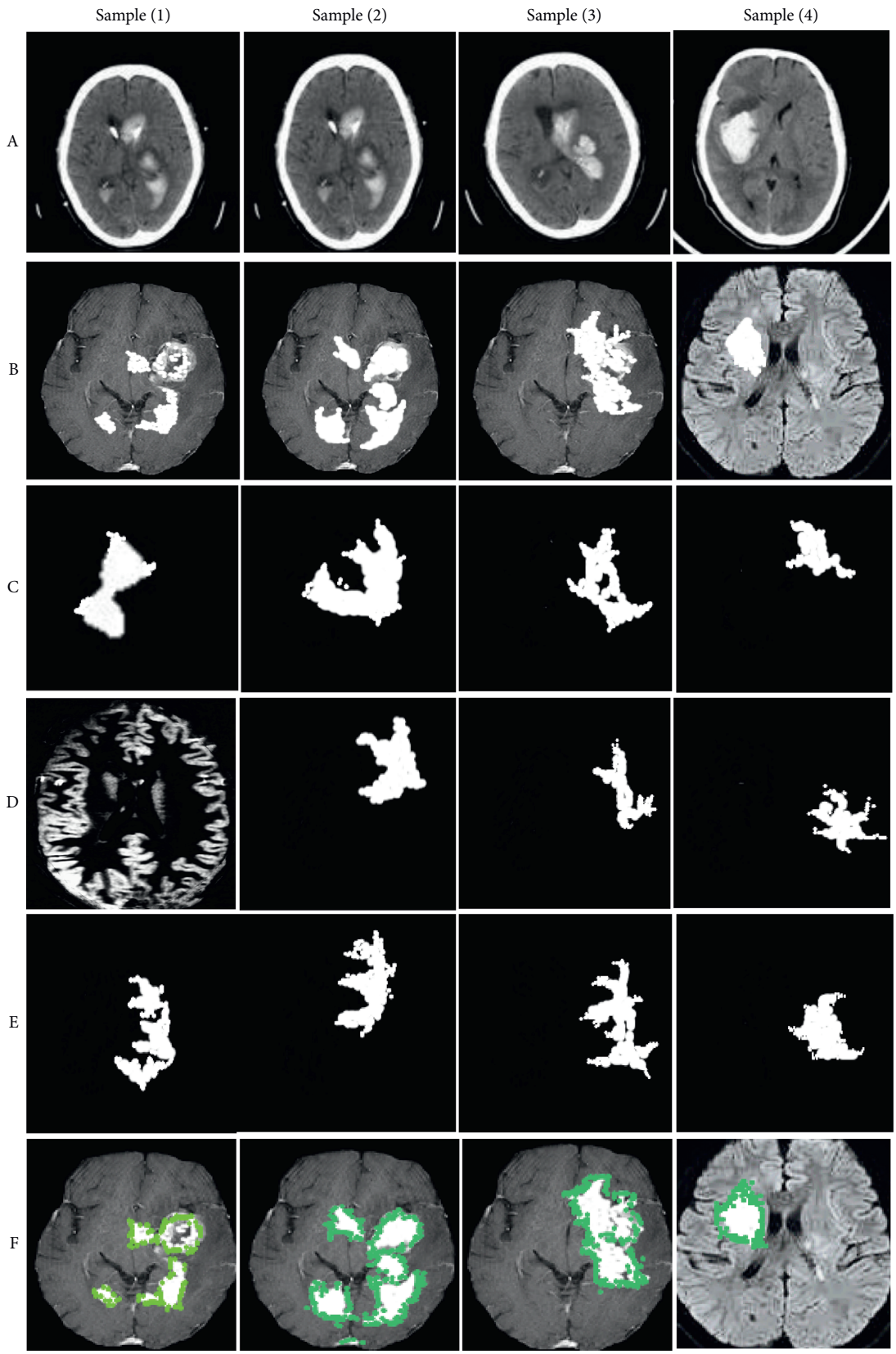

Figure 8: Brain CT image segmentation results of each algorithm. (A) original CT images; (B) intracranial tissue images; (C) threshold segmentation results; (D) FCM algorithm segmentation results; (E) FCRLS algorithm initialization results; (F) DRLSRE model iterative evolutionary segmentation results.

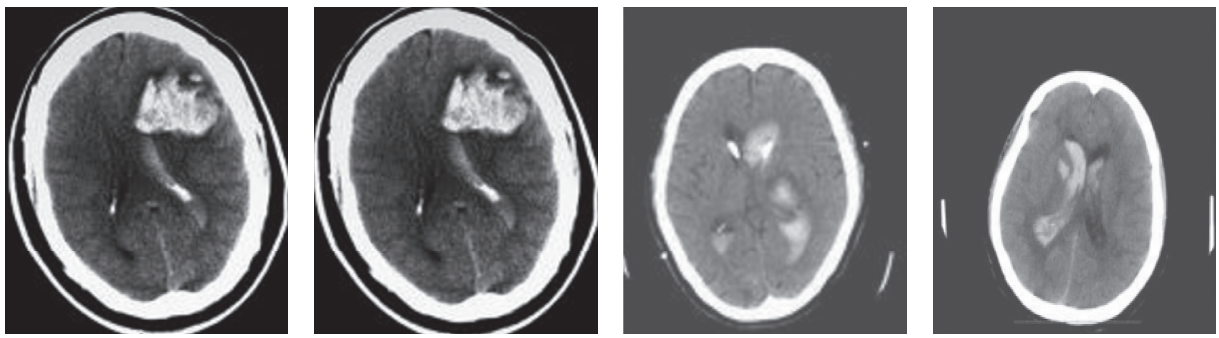

(a) (b) (c) (d)

Figure 9: CT of each bleeding level of the patient. (a) Bleeding level 1. (b) Bleeding level 2. (c) Bleeding level 3. (d) Bleeding level 4.

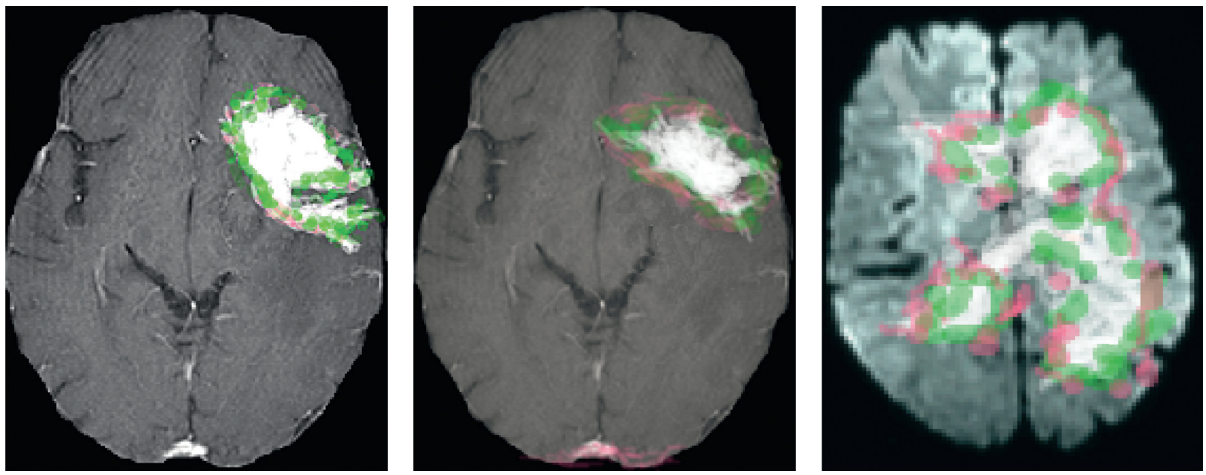

(a) (b) (c)

Figure 10: FCRLS algorithm segmentation results. (a) Bleeding level 1. (b) Bleeding level 2. (c) Bleeding level 3.

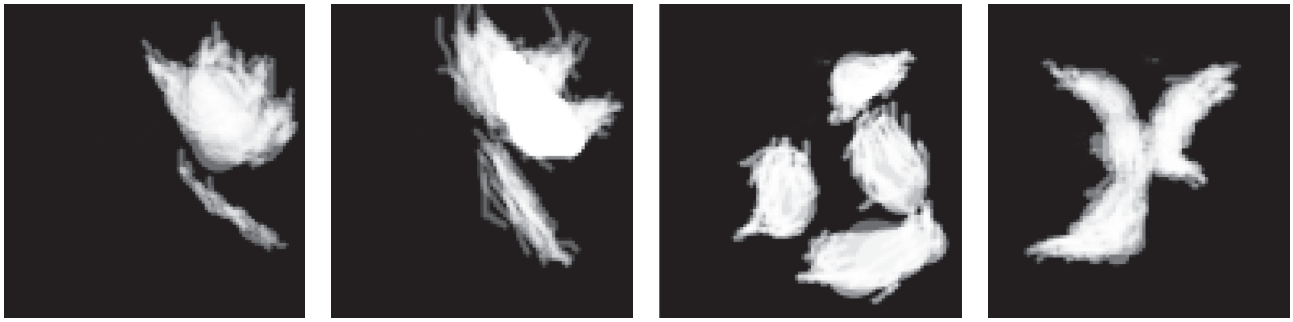

(a) (b) (c) (d)

Figure 11: Final binarization processing results. (a) Bleeding level 1. (b) Bleeding level 2. (c) Bleeding level 3. (d) Bleeding level 4.

experienced physicians, it was found that when the number of iterations of the level function was 200, 300, 400, and 500, respectively, the segmentation results of the four groups of cases by each algorithm were the closest to the real lesion area. In addition, the FCRLS algorithm for segmentation of CT images of inconspicuous, irregular, and discontinuous cerebral hemorrhage was more dominant over other algorithms.

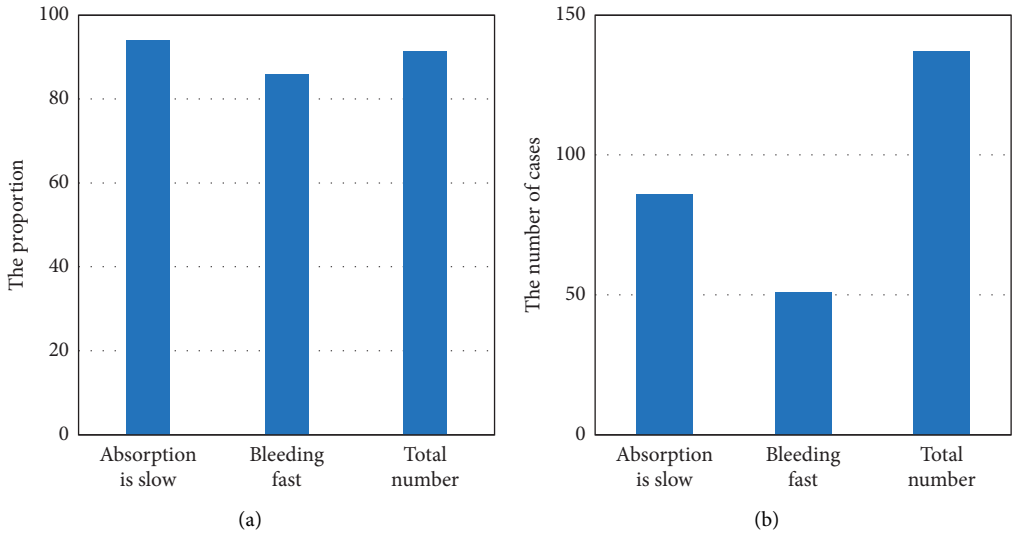

Figure 12: The correct rate of prediction of hematoma absorption by the system. The graph of (a) each value and (b) the proportion.

3.2. Example of Calculation of Blood Volume in Patients with Cerebral Hemorrhage. Patient A was taken as an example to demonstrate the calculation results of bleeding volume. The basic CT images, segmentation results, and final binary segmentation results of Patient A are shown in Figures 9–11, respectively. For patients with irregular and discontinuous bleeding at A1, 2, and 3 levels, FCRLS algorithm was utilized to segment the segmentation results, as shown in Figure 9. Then, binarization processing was carried out. A region-based threshold segmentation algorithm was adopted for the four levels of the patient, and the final binarization results of all levels of the patient are shown in Figure 11. The bleeding area of each level was counted as follows: level 1, 8.0213 cm^2; level 2, 10.234 cm^2; level 3, 10.435 cm^2; level 4, 1.7112 cm^2. The total bleeding volume is calculated as follows: $VA = (8.0213 + 10.234 + 10.435 + 1.7112\,cm^2) * 1\,cm = 30.4015\,mL$.

3.3. Hematoma Absorption Prediction Effect. Figure 12 shows the correct rate of the system for predicting the absorption of the patient's hematoma. 150 effective cases were predicted. Among 91 patients with a slow absorption rate of hematoma, 86 predictions were correct, and the prediction accuracy was 94%. In 59 patients with slow absorption of hematoma, 51 cases were correct, and the correct rate of prediction was 86%. The overall prediction accuracy was 91.3%. Therefore, CAD system has a high adoption prospect and value in the diagnosis and treatment of hypertensive intracerebral hemorrhage. The system was accurate in predicting the condition of patients with hematoma, especially for patients with slow hematoma bleeding, and had certain clinical value.

4. Discussion

Hypertensive intracerebral hemorrhage is a common cerebrovascular disease that poses a high threat to human health worldwide. Cerebral blood vessels in hypertensive patients generally have fibrous and hyaline lesions, which will further cause local vascular necrosis and dilation, but cerebral hemorrhage will occur when blood pressure changes greatly [13]. It means that anything that can cause changes in blood pressure can cause a brain hemorrhage. This is also the reason for the frequent occurrence of hypertensive intracerebral hemorrhage [14]. The number of patients with intracerebral hemorrhage caused by hypertension admitted to our hospital is increasing year by year, and the causes of hemorrhage are basically the same as previous studies.

Brain CT is an important tool for diagnosis and treatment of hypertensive intracerebral hemorrhage. Clinicians generally judge and analyze the bleeding site, amount of bleeding, midline displacement, degree of ventricular compression, and other information based on the patient's CT images to further decide whether the patient needs surgery [15]. At present, the patient's blood loss in domestic hospitals is manually calculated according to the traditional Tada equation. This method has the disadvantages of cumbersome, large error, and low efficiency. In addition, doctors analyze CT images according to their own experience to further analyze the patient's condition, which is prone to large errors, such as omission and misdiagnosis, and also prone to large differences in the judgment structure between different doctors. With the continuous maturity and deepening of the adoption of Internet technology, computer-aided diagnostic medicine has been developed. The research in this field is more advanced abroad than in China. For example, the 3D slicer software has launched version 4.2 in 2012 [16]. The software is not restricted by the bleeding site and hematoma shape, and its adoption is gradually mature. Domestic research studies mainly focus on the calculation of hematoma volume and blood loss. Some scholars proposed CT volumetric measurement and other methods to calculate hematoma volume, which improved the diagnostic efficiency and accuracy [17, 18]. However, all operations need to be performed on CT, which makes the operation complicated. Researches in this field are mostly theoretical, and problems such as poor clinical

applicability and relatively simple function are prevalent [19, 20]. In this work, based on the study data of CT images of patients with hypertensive hemorrhage, a CAD system was proposed and verified in practice based on machine learning. The results showed that the system proposed can comprehensively and accurately obtain the information of bleeding site, bleeding volume, midline displacement, and ventricle compression degree. An accurate assessment of hematoma bleeding can also be made. It can be utilized as an auxiliary means of doctor's diagnosis and treatment and has high clinical adoption value.

5. Conclusion

In this work, based on the study data of CT images of patients with hypertensive hemorrhage, a CAD system was proposed and verified in practice based on machine learning. Acute intracerebral hemorrhage is a series of acute clinical symptoms caused by the rapid rupture of cerebrovascular soil. They often show symptoms such as severe headache, vomiting, limb paralysis, and even coma. Chronic intracerebral hemorrhage generally refers to the pathological changes of blood vessel itself, or the pathological changes of blood system itself, leading to the disorder of blood coagulation mechanism of patients, mild rupture of cerebrovascular, slow bleeding speed, long bleeding time, or intracerebral hemorrhage caused by hemodialysis for a long time in brain tissue. The study results showed that the system proposed could comprehensively and accurately obtain the information of bleeding site, bleeding volume, midline displacement, and ventricle compression degree, and the segmentation of lesions was also very fast and accurate. Moreover, an accurate assessment of hematoma bleeding was made. In conclusion, the proposed CAD system can be utilized as an auxiliary means of doctor's diagnosis and treatment and is of high clinical adoption value.

Data Availability

The data used to support the findings of this study are available from the corresponding author upon request.

Conflicts of Interest

The authors declare no conflicts of interest.

References

[1] W. C. Ziai, C. B. Thompson, S. Mayo et al., "Intracranial hypertension and cerebral perfusion pressure insults in adult hypertensive intraventricular hemorrhage," *Critical Care Medicine*, vol. 47, no. 8, pp. 1125–1134, 2019.

[2] I. C. Hostettler, D. J. Seiffge, and D. J. Werring, "Intracerebral hemorrhage: an update on diagnosis and treatment," *Expert Review of Neurotherapeutics*, vol. 19, no. 7, pp. 679–694, 2019.

[3] W. Ding, Z. Gu, D. Song, J. Liu, G. Zheng, and C. Tu, "Development and validation of the hypertensive intracerebral hemorrhage prognosis models," *Medicine (Baltimore)*, vol. 97, no. 39, Article ID e12446, 2018.

[4] A. L. de Oliveira Manoel, "Surgery for spontaneous intracerebral hemorrhage," *Critical Care*, vol. 24, no. 1, p. 45, 2020.

[5] S. Xu, B. Du, A. Shan, F. Shi, J. Wang, and M. Xie, "The risk factors for the postoperative pulmonary infection in patients with hypertensive cerebral hemorrhage," *Medicine (Baltimore)*, vol. 99, no. 51, Article ID e23544, 2020.

[6] A. Tan, S. Costi, L. S. Morris et al., "Effects of the KCNQ channel opener ezogabine on functional connectivity of the ventral striatum and clinical symptoms in patients with major depressive disorder," *Molecular Psychiatry*, vol. 25, no. 6, pp. 1323–1333, 2020.

[7] H. Gilutz, S. Shindel, and I. Shoham-Vardi, "Adherence to NSTEMI guidelines in the emergency department," *Critical Pathways in Cardiology: Journal of Evidence-Based Medicine*, vol. 18, no. 1, pp. 40–46, 2019.

[8] F. Mold, M. Raleigh, N. N. Alharbi, and S. de Lusignan, "The impact of patient online access to computerized medical records (CMR) and services for Type 2 Diabetes: systematic review. (Preprint)," *Journal of Medical Internet Research*, vol. 20, no. 7, Article ID e235, 2018.

[9] K. Seevnarain, N. Burke, and K. Newbigin, "Case series analysis of eight underground tunnellers with chronic silicosis in Queensland," *Respirology Case Reports*, vol. 9, no. 6, Article ID e00756, 2021.

[10] Z. Lv, X. Li, and W. Li, "Virtual reality geographical interactive scene semantics research for immersive geography learning," *Neurocomputing*, vol. 254, pp. 71–78, 2017.

[11] K. Watson, R. Broscious, S. Devabhakthuni, and Z. R. Noel, "Focused update on pharmacologic management of hypertensive emergencies," *Current Hypertension Reports*, vol. 20, no. 7, p. 56, 2018.

[12] O. Matz, A. Arndt, J. Litmathe, M. Dafotakis, and F. Block, "Risikofaktoren für hypertensive und zerebrale Amyloidangiopathie-assoziierte intracerebrale Blutungen: ein retrospektiver Vergleich," *Fortschritte der Neurologie - Psychiatrie*, vol. 86, no. 12, pp. 763–769, 2018.

[13] G. Sun, X. Li, X. Chen, Y. Zhang, and Z. Xu, "Comparison of keyhole endoscopy and craniotomy for the treatment of patients with hypertensive cerebral hemorrhage," *Medicine (Baltimore)*, vol. 98, no. 2, Article ID e14123, 2019.

[14] Y. S. Hori, T. Ohkura, Y. Ebisudani et al., "Hypertensive cerebral hemorrhage in a patient with turner syndrome caused by deletion in the short arm of the X chromosome," *Pediatric Neurosurgery*, vol. 53, no. 3, pp. 167–170, 2018.

[15] S. Hu, Q. Ma, B. Li, Q. Wu, and R. Han, "Association of hypothyroidism with hypertensive intracerebral hemorrhage: a case-control study," *World Neurosurgery*, vol. 134, pp. e8–e11, 2020.

[16] Y. Zhang, L. Song, and J. Zhao, "Role of scalp hypothermia in patients undergoing minimally invasive evacuation of hypertensive cerebral hemorrhage," *Pakistan Journal of Medical Sciences*, vol. 35, no. 5, pp. 1451–1455, 2019.

[17] W. Xuejian, Y. Chen, Z. Wang, and M. Qian, "Clinical research of early hyperbaric oxygen therapy on patients with hypertensive cerebral hemorrhage after craniotomy," *Turkish Neurosurgery*, vol. 30, no. 3, pp. 361–365, 2019.

[18] S. Zhang, X. Zhang, Y. Ling, and A. Li, "Predicting recurrent hypertensive intracerebral hemorrhage: derivation and validation of a risk-scoring model based on clinical characteristics," *World Neurosurgery*, vol. 127, pp. e162–e171, 2019.

[19] Y. Sun, B. Xu, and Q. Zhang, "Nerve growth factor in combination with oxiracetam in the treatment of hypertensive cerebral hemorrhage," *Pakistan Journal of Medical Sciences*, vol. 34, no. 1, pp. 73–77, 2018.

[20] M. Pasi, L. Sugita, L. Xiong et al., "Association of cerebral small vessel disease and cognitive decline after intracerebral hemorrhage," *Neurology*, vol. 96, no. 2, Article ID e192, 2021.